Element-specific channels for the photoexcitation of V-doped TiO_2 nanoparticles

Giacomo Rossi,[1] Marco Calizzi,[1] Lucia Amidani,[2] Andrea Migliori,[3] Federico Boscherini,[1,4,*] and Luca Pasquini[1]

[1]*Department of Physics and Astronomy and CNISM, University of Bologna, Viale C. Berti Pichat 6/2, 40127, Bologna, Italy*

[2]*ESRF – The European Synchrotron, CS40220, 38043 Grenoble, France*

[3]*Consiglio Nazionale delle Ricerche, Istituto per la Microelettronica e i Microsistemi, Bologna, Italy*

[4]*Consiglio Nazionale delle Ricerche, Istituto Officina dei Materiali, Strada Statale 14, Km. 163.5 in AREA Science Park, 34149 Basovizza, Trieste, Italy*

(Received 20 February 2017; revised manuscript received 1 June 2017; published 7 July 2017)

Incorporation of dopants in semiconductors is commonly used to modify the optical response and improve the efficiency of related devices. A physical understanding with elemental and local sensitivity of the electron excitation and trapping channels which follow photoexcitation is a prerequisite for knowledge-based materials design. By using high-resolution x-ray absorption methods we show that, in V-doped TiO_2 nanoparticles, subband-gap visible light absorption is predominantly due to excitation of electrons from V ions to defective and long-lived Ti sites. We thus identify an element-specific photoexcitation channel.

DOI: 10.1103/PhysRevB.96.045303

I. INTRODUCTION

Doping—incorporation of a small quantity of a foreign atomic species—is a well-known tool to modify the physical properties of semiconductors and insulators. Depending on the system, the dopant may be incorporated in a substitutional site in the host matrix or may form complexes involving considerable lattice relaxation, such as dopant clusters and dopant-vacancy complexes. Dopants can change the optical properties by introducing states in or near the forbidden energy gap and can modify the transport properties by releasing charge carriers and/or giving rise to traps which reduce the carrier lifetime. The modification of the optical properties may be due to various phenomena, including excitation of electrons from dopant states in the gap to the host conduction band and/or excitation of host electrons from the valence band to defect gap states induced by the dopants. A physical description and understanding of these aspects is crucially important.

Generation of electrons and holes by visible or near-visible light absorption in semiconductor nanostructures plays a crucial role in photoelectrochemistry and photocatalysis. These charges, once they are found on the surface of a nanoparticle, make oxidation and reduction processes possible, with applications such as hydrogen production from water, environmental cleaning (air and water), dye-sensitized solar cells, and others [1]. In all these processes, the charge carriers undergo many elementary steps, including initial generation by light absorption, scattering, trapping, possible recombination in the "bulk" at defect sites prior to reaching the surface, and trapping on surface sites. Each of these steps affects the efficiency of a real device. Clearly, to go beyond a trial-and-error approach, a physical description and understanding of each of these steps is of great importance and may lead to knowledge-based materials and device design and engineering.

Titanium dioxide (TiO_2), especially in the form of nanoparticles (NPs), is one of the most studied oxide semiconductors for photocatalysis. However, because of its wide band gap (≈3.2 and 3.0 eV in anatase and rutile polymorphs, respectively), only a small fraction of the solar spectrum is harvested, i.e., UV light (3%–5% of total). The incorporation of 3*d* transition metals is an effective approach to decrease the band gap and to improve visible light photocatalytic activity [2]. Band-gap reduction is the result of the creation of states in the band gap of the matrix, as systematically investigated theoretically by Umebayashi *et al.* [3]. They found that V, Cr, Mn, Fe, and Co create donor states, their positions shifting towards the valence band with increasing atomic number; V, the subject of the present paper, was predicted to create a gap state near the bottom of the conduction band. Their findings are in agreement with various other predictions [4,5]. While it is generally accepted that V acts as a donor dopant, the specific mechanism(s) which enhance visible light absorption are unclear. As also noted by Choi *et al.* [6], it is unclear whether band-gap reduction is due to electron excitation from dopant states in the gap to the host conduction band or to transitions from the host valence band to defect states in the gap, possibly also related to oxygen vacancies induced by the presence of dopants, or both. The open questions are: (i) Does light absorption lead to the release of an electron from V or the opposite? (ii) If an electron is, in fact, released from V, what is its fate, that is, is it transferred to the TiO_2 matrix on a particular atomic site (Ti or O, bulk or surface)?

In this paper, we shed light on the above issues by using high-energy-resolution fluorescence detected x-ray absorption near edge structure (HERFD-XANES) under differential visible light illumination. In fact, x-ray absorption spectroscopy (XAS) is one of the premier tools to study the location of dopants in semiconductors [7]. Recent variations and improvements in XAS-related methods, especially the high-resolution analysis of the emitted photon spectrum [8], have added a new level of refinement and sensitivity for both static and dynamic studies. HERFD-XAS can be used to study charge-transfer processes, as shown by the recent study by

*Corresponding author: federico.boscherini@unibo.it

some of us of hot electron transfer from Au to TiO_2 NPs induced by plasmon excitation in the metal [9]. As for the specific system investigated, we have recently demonstrated that V dopants in TiO_2 NPs are found in both 4+ and 5+ oxidation states in bulk and surface sites, respectively, and occupy substitutional sites irrespective of whether the matrix has an atomic structure similar to rutile or anatase [10]. Now, we use V $K\alpha$– and Ti $K\beta$-detected HERFD-XANES under differential illumination to demonstrate that visible light absorption predominantly leads to electron transfer from V to long-lived Ti-related traps.

II. SAMPLE DEPOSITION AND CHARACTERIZATION

Samples studied in the present paper consisted of V-doped TiO_2 (V : TiO_2) NPs deposited by gas-phase condensation in a He atmosphere [10,11]. Ti and V powders were mixed, heated under vacuum in a W evaporation crucible above the melting point of Ti (1668 °C), rapidly cooled down to about 1200 °C, and left to homogenize for 2 hours. Subsequently, evaporation slightly above the melting point under a He pressure of 266 Pa was monitored by a quartz crystal microbalance while the NPs were deposited on a rotating steel cylinder cooled by liquid nitrogen. After the deposition, high vacuum was restored in the chamber and the NPs were oxidized by admitting O_2 up to a final pressure of 2.6 kPa. The V content in the samples, expressed as the relative fraction of V/(Ti + V) atoms, was determined by energy-dispersive x-ray spectroscopy (EDS) in a Leica Cambridge S360 scanning electron microscope. Samples were crystallized by annealing in air at 400 °C for 8 hours.

Samples were characterized by a range of in-house methods, including optical spectroscopy, powder x-ray diffraction (XRD), and transmission electron microscopy (TEM). XRD patterns were recorded with a Panalytical X'Celerator powder diffractometer using Cu $K\alpha$ radiation. Figure 1 displays the XRD patterns of samples A and B, which clearly reveal the presence of both rutile and anatase. The weak and broad reflection at around 31° indicates that both samples contain a small amount of brookite, while Bragg reflections attributable

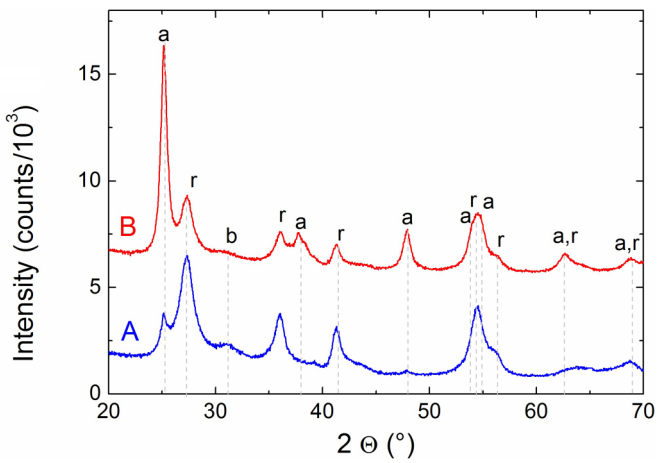

FIG. 1. XRD patterns of samples A and B, vertically shifted for the sake of clarity. The Bragg reflections of rutile (r), anatase (a), and brookite (b) are indicated.

TABLE I. Phase composition (a = anatase, b = brookite, r = rutile) determined by XRD analysis, and V content measured by EDS for the two V : TiO_2 NPs samples. Uncertainties expressed as 1 standard deviation on the least significant digit are given in brackets.

Sample	Composition (wt %) A	B	R	V/(Ti+V) (at %)
A	10 (2)	10 (2)	80 (4)	3.0 (5)
B	43 (3)	10 (2)	47 (3)	3.5 (5)

to vanadium oxides were not detected; no oxide phases where detected by TEM and Raman spectroscopy. Table I lists the relative phase abundances determined by Rietveld refinement of XRD patterns using the program MAUD [12]. While sample A is constituted mainly of rutile (80%) with anatase and brookite as minority phases, in sample B anatase and rutile exhibit similar weight fractions. Analysis of the peak broadening yields a crystallite size of about 15 nm.

Figure 2 (top) shows a TEM image of sample B taken with a FEI TECNAI F20 microscope operating at 200 kV. For TEM investigations, NP powders were dispersed in ethanol, sonicated, and drop cast on a holey carbon supported by a copper grid. The NP size ranged between 8 and 18 nm. The mean NP size is (12 ± 1) nm estimated on a statistical sample of 80 particles. The close similarity of NP size and crystallite size determined by XRD indicates that most NPs are constituted of one single crystal. The NP ensemble displays a highly interconnected morphology resulting from NP aggregation, both in the gas phase and on the collection substrate. The high-resolution TEM (HR-TEM) images in Fig. 2 (bottom) and their Fast-Fourier transforms (FFTs) show the coexistence of rutile and anatase TiO_2 polymorphs on a ∼10-nm scale. This peculiar phase distribution results in a large number of both homophasic and heterophasic interfaces in the samples.

X-ray spectroscopy measurements were performed at the ID26 beamline of the ESRF, Grenoble, France; use of analyzer crystals was essential to separate V and Ti emission lines. We discuss: (i) XANES spectra at the Ti K edge obtained in the total fluorescence yield (TFY) mode [13]; (ii) V 1s valence-to-core x-ray emission spectra (vc-XES) [13]; (iii) resonant inelastic x-ray scattering (RIXS) measurements in the vicinity of the V $K\alpha$ emission lines; and (iv) HERFD-XANES spectra obtained by measuring the intensity of the Ti $K\beta$ and V $K\alpha$ emission as a function of the impinging photon energy, both in the static and in the differential illumination mode, as described below. For HERFD-XANES the incident beam energy was selected with a Si(311) double-crystal monochromator and tuned to Ti and V K edges. Higher harmonics were rejected by three Si mirrors in total external reflection at 2.5 mrad. The emission spectrometer of ID26, based on Bragg optics arranged in Rowland geometry, was equipped with five Ge(331) bent ($R = 1$ m) crystal analyzers and tuned between 75.58° and 74.70° to analyze alternatively Ti $K\beta$ and V $K\alpha$ emission lines. The combined resolution of monochromator and spectrometer was 0.7 eV. Samples were measured as compacted powders mounted on transparent tape. All measurements were performed at room temperature and in air.

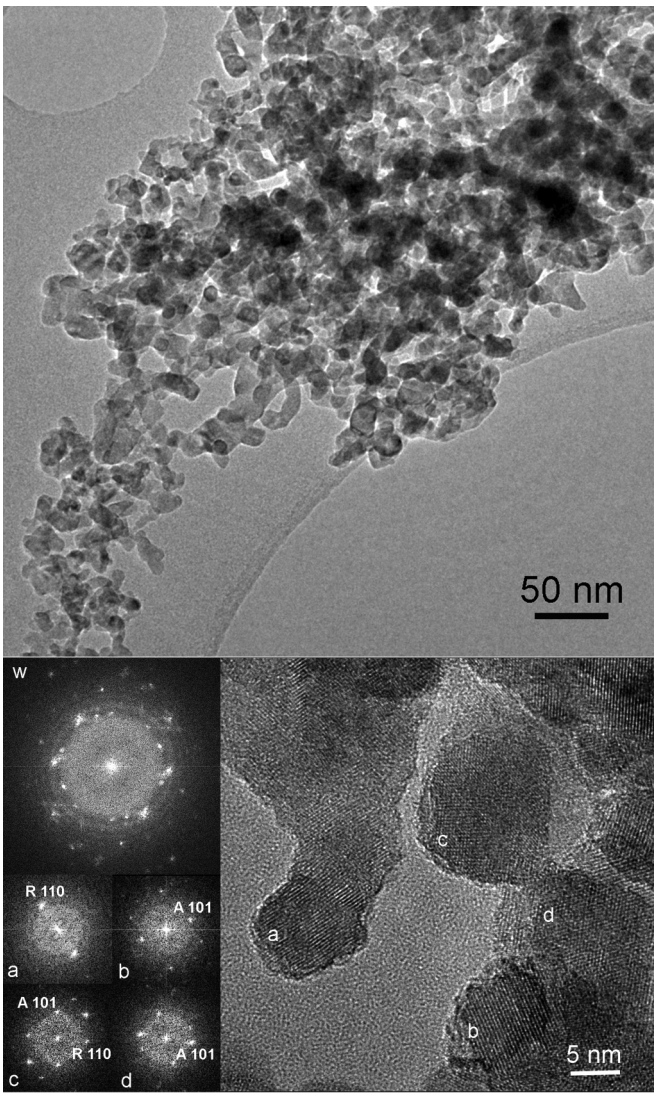

FIG. 2. (Top) TEM image of sample B; (Bottom) HR-TEM image and the corresponding FFTs performed on the whole micrograph (w) and on the grains labeled by lowercase letters. This image shows the intimate coexistence of the rutile (R) and anatase (A) on a few-nanometers scale, as it is clearly indexed in the FFT patterns.

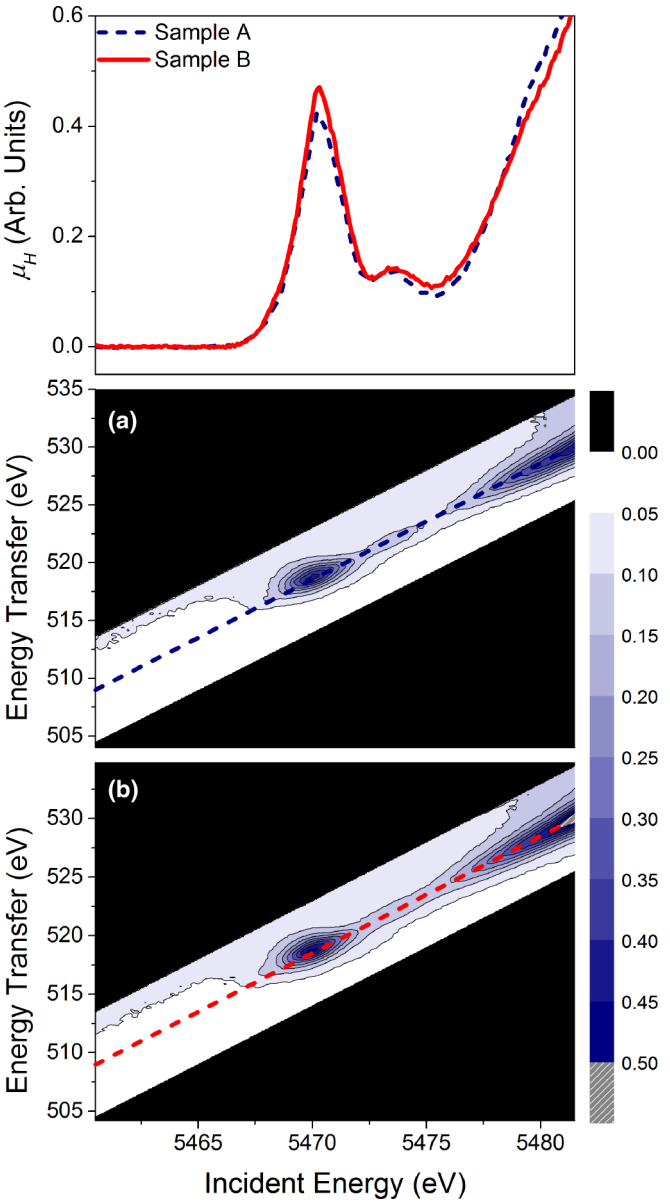

FIG. 3. Bottom two panels: V $K\alpha$ RIXS planes for both samples in the pre-edge region; Top panel: corresponding HERFD-XANES spectra obtained by measuring the scattered intensity along the dashed lines in the RIXS planes.

Selected HERFD - XANES spectra at both the V and Ti edges were recorded with and without illumination by a 532-nm, continuous-wave 200 mW laser diode focused in a 1.2 mm^2 circular spot. In order to record small photoinduced changes, we chose to measure a high number ($\sim$100) of cycles, each consisting of one HERFD-XANES spectrum under illumination and one without, each lasting 1 min; this procedure minimizes various experimental artifacts. Laser-induced sample heating was less than 3 °C. The reproducibility of the energy axis was checked by comparing the position of a clearly identifiable pre-edge feature over 100 spectra collected under the same illumination conditions. The resulting standard deviation of the mean was less than 5 meV, which is more than an order of magnitude lower than the observed laser-on/laser-off shift that is discussed later on. This ensures the authenticity of the laser-induced effects. Differential spectra were calculated by subtracting the sum of laser-off spectra from the sum of the laser-on spectra. For each spectrum the following processing steps were performed: normalization to the intensity of the incoming beam, averaging of the scans to increase the signal-to-noise ratio, subtraction of the pre-edge region (estimated as a linear fit in the regions 5450–5460 eV for V and 4950–4960 eV for Ti spectra), and normalization to the average value in the postedge region (between 5015 and 5035 eV for Ti spectra and between 5520 and 5550 eV for V spectra). The whole procedure was performed using PYMCA [14].

In Fig. 3 we report the V $K\alpha$ RIXS planes for both samples in the pre-edge region and the corresponding HERFD-XANES spectra (indicated as μ_H, in which the subscript H indicates "high resolution") obtained by measuring the scattered intensity along the indicated dashed lines in the

RIXS planes. The spectral features are related to transitions involving dipole and quadrupole transitions to bound orbitals derived from O p and V d atomic ones. The HERFD-XANES spectra are similar to "conventional" XANES recorded on similar samples which demonstrated that V is substitutional to Ti [10]; the present spectra, however, exhibit sharper spectral features due to the use of the crystal analyzers and allow a higher level of refinement. In fact, XANES spectra may not be able to detect weak spectral features, which could indicate the presence of multiple sites or local distortions. This is especially true when weak features appear off the main diagonal of the RIXS plane. The RIXS planes reported in Fig. 3 confirm that the pre-edge consists of a main peak and a weak shoulder and that their maxima lie on the diagonal of the RIXS plane. All V K-edge HERFD-XANES were thus acquired at the emission energy corresponding to the diagonal of the RIXS plane. We note that data reported in Fig. 3 are very similar to those reported by Bordage [15] on V-doped TiO_2 nanowires synthesized by chemical methods. Both the RIXS planes and the HERFD-XANES spectra of sample B exhibit slightly broader features compared to sample A; this is compatible with the presence of both rutile and anatase polymorphs in sample B, while rutile is dominant in sample A. The common conclusion of the above analysis and the Ti XANES and vc-XES reported in the Supplemental Material [13] is that in both samples V is a substitutional dopant that occupies the cationic site, irrespective of the structure of the matrix (rutile or mixed). This forms the structural framework upon which we base the study of the electron transfer process as reported below.

III. ELECTRON TRANSFER PROCESS

In the top row of Fig. 4 we report the HERFD-XANES spectra with and without illumination for the two samples at both Ti and V edges. In the mid and bottom rows, we display as dots the corresponding experimental differential HERFD-XANES spectra $\Delta\mu_H \equiv \mu_H{}^{\text{on}} - \mu_H{}^{\text{off}}$. It is quite clear that light absorption causes significant changes in the spectra, which are well above the noise level. In particular, light absorption leads to a significant shift to higher energies of the main absorption edge of V while the opposite occurs at the Ti edge (insets in the top row panels); this is reflected in the opposite sign of the differential spectra in the regions 5475–5490 eV (negative for V) and 4975–4985 eV (positive for Ti), highlighted in the figure with the vertical arrows. This effect is

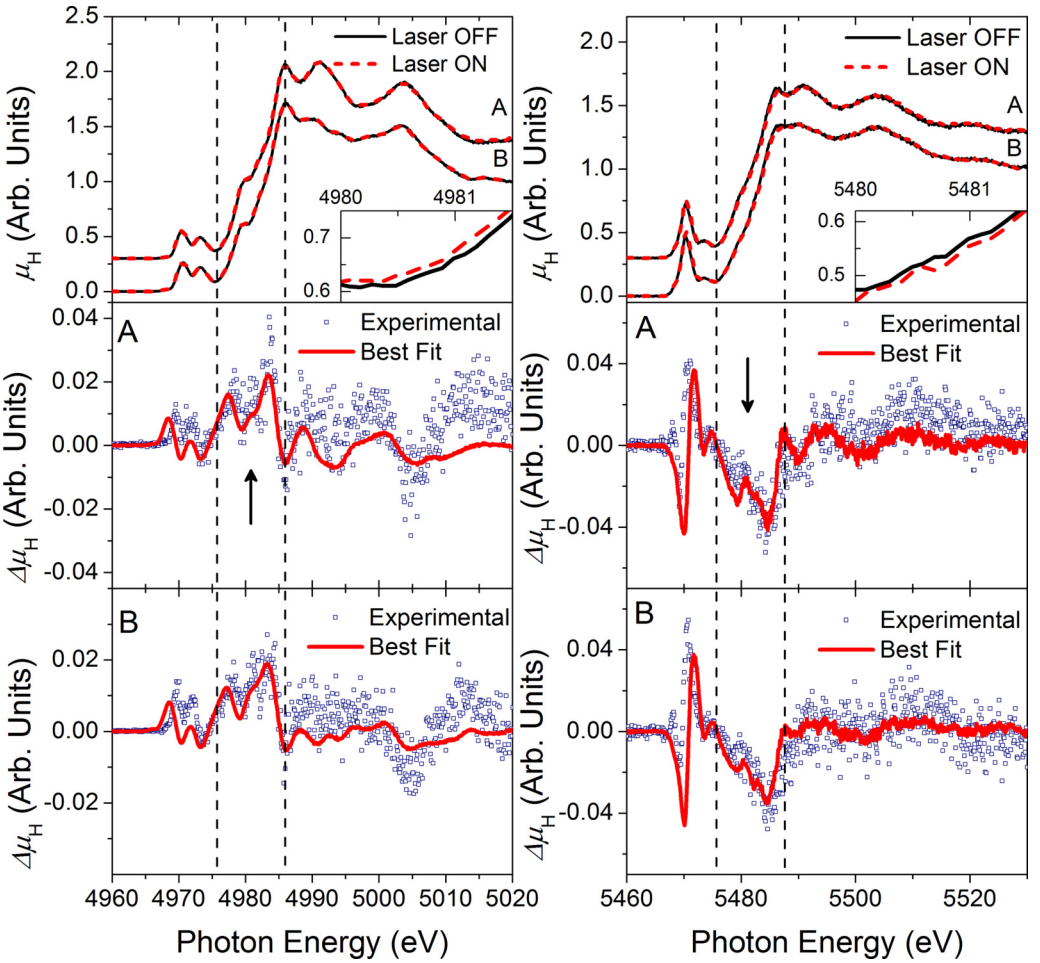

FIG. 4. Top row: HERFD-XANES spectra μ_H for samples A and B with and without laser illumination; the inset is a zoom on the rising edge, highlighting the edge shift. Middle and bottom panels: differential HERFD-XANES spectra $\Delta\mu_H$ and best fit obtained as described in the text. In all cases, left column Ti $K\beta$ HERFD-XANES, right column V $K\alpha$ HERFD-XANES.

fully reproducible in each laser-on/laser-off cycle and is fully reversible, since the same spectral changes were found for each of the 100 cycles of laser-on/laser-off spectra, implying no laser-induced damage. The most plausible explanation for this observation is that light absorption predominantly leads to electron transfer from the V dopant to the Ti atoms in the host matrix, equivalent to a transient oxidation of V cations and a reduction of Ti ones. We note that illumination of undoped TiO_2 under very similar conditions and the same experimental setup was found to give rise to no discernible effect, as also previously reported [9].

Following previous studies [9,16] of photoinduced effects on XAS spectra we modeled the differential spectra $\Delta\mu_H(\hbar\omega)$ by an edge-shift approach, according to the equation

$$\Delta\mu_H(\hbar\omega) = \xi\{\mu_H{}^{\text{off}}(\hbar\omega - \Delta E) - \mu_H{}^{\text{off}}(\hbar\omega)\},$$

in which $\mu_H{}^{\text{off}}(\hbar\omega)$ is the HERFD-XANES laser-off spectrum, the energy shift ΔE accounts for the effect of charge transfer, and the multiplicative coefficient ξ represents the fraction of V or Ti atoms in the photoexcited state. We then implemented a least-squares fitting routine to minimize the difference between the experimental and calculated differential spectrum, using the edge shift and the excited-state fraction as fitting parameters. The fitting was performed in the main edge ranges (i.e., 4974–5020 eV for Ti and 5474–5520 eV for V), which correspond to transitions to continuum unbound states. In all cases, good fits were found with values of the reduced χ^2 merit function [17] at minimum lower than 0.5; the fits for Ti edge spectra above 4990 eV, a region characterized by a higher noise level and thus giving a smaller contribution to χ^2, are of lower quality. However, we found that there was a significant correlation between the fitting parameters, leading to a rather wide range of values which gave acceptable fits (with respect to the best fit values about ± 1 eV for the edge shifts and about ± 0.2 for the excited state fraction). Therefore, we chose to fix the edge shifts for the V and Ti spectra to literature values corresponding to the edge shift between V^{4+} and V^{5+} and between Ti^{4+} and Ti^{3+}, respectively. Following this approach, we used edge shifts of $+1.0$ eV for the V-edge spectra [18,19] (equal to the difference in main edge energy between VO_2 and V_2O_5) and -2.0 eV for Ti ones [20] (average difference in spectral features between rutile TiO_2 and α-Ti_2O_3); these values of edge shifts are within 0.1 eV of the best fit ones. Clearly, fixing the edge shifts to those corresponding to reference compounds is an approximation, since they refer to compounds in which not only there is a change of the oxidation state but also of the local structure (typically with a difference in coordination geometry). A structural change affects the overall XANES line shape, but in a first approximation it is reasonable that the dominant effect comes from the different oxidation state. Having fixed the edge shifts, the best estimates of the excited-state fractions were found from the fitting routine. The best fits are reported as the continuous red lines in Fig. 4 and clearly reproduce quite well the experimental observations. With the parameters used to fit the main edge regions some discrepancies were found in the pre-edge regions of the spectra. This is not surprising because the pre-edge features correspond to transitions to more localized states than in the main edge, and thus they are differently affected by the light-induced electron transfer;

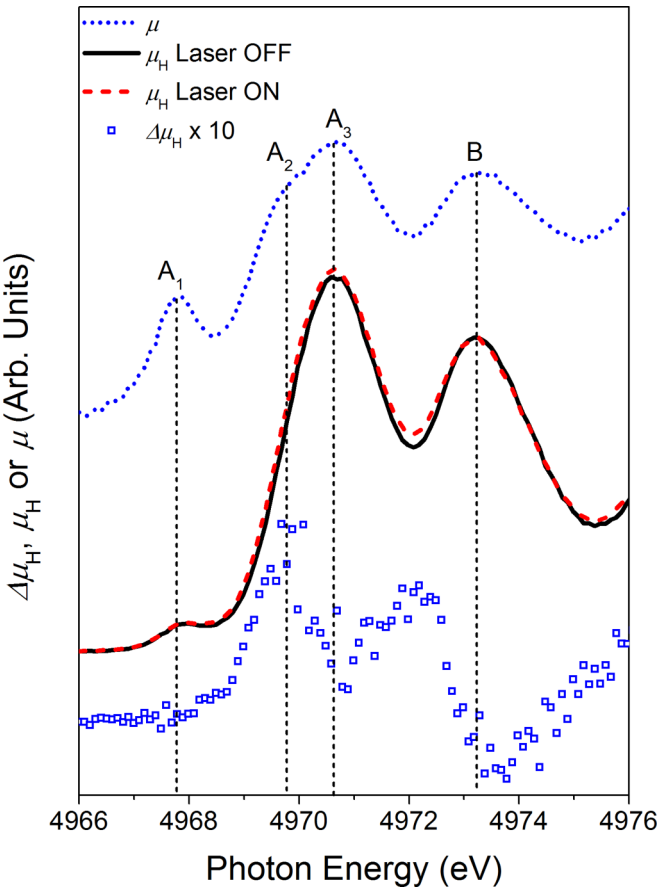

FIG. 5. The continuous lines report the Ti $K\beta$ HERFD-XANES spectra with and without illumination in the region of the pre-edge peaks for sample B. The bottom empty dots correspond to the difference curve multiplied by a factor of 10. The top dashed line is the spectrum recorded in the TFY mode, as a reference.

hence, different energy shifts might be necessary to reproduce the differential spectra in the pre-edge and main edge region. Estimates of the uncertainties in the excited-state fractions were obtained using standard statistical analysis methods [17] considering the noise in the data and the range of excited-state fractions for which $Q(\frac{N-2}{2}, \frac{\chi^2}{2}) > 0.1$, in which N is the number of experimental points and Q is the incomplete γ function. In this way, for samples A and B we found the values of excited-state fractions equal to $20\% \pm 10\%$ for V and $3.5\% \pm 1.5\%$ for Ti. We regard these values as indicative and, given the approximations, acceptable as a rough estimate.

Further insight on the trapping site on Ti cations is provided by analysis of the HERFD-XANES difference curves in the region of the Ti pre-edge peaks, reported in Fig. 5 for sample B; very similar spectra were recorded for sample A. While there are line-shape changes over the full pre-edge region, one of the strongest features in the difference curves is in the region of the A_2 feature, which is known to be related to low-coordinated defective Ti sites [21–25]. An increase of this feature has been observed in previous studies of electron transfer processes in nanostructured TiO_2 systems [9,16], suggesting that absorption of light and charge transfer induces the creation of low-coordinated defective

Ti sites. We conclude that a similar effect occurs also in V : TiO_2.

The excited-state fraction of V atoms can provide an order-of-magnitude estimate for the lifetime of the excited trapped state. We assume a two-level model in which V can be in the ground or excited state and in which transition rates from one to the other are determined by the characteristic times τ_{ge} and τ_{eg}. In general, the derivative of the excited-state fraction n_e is

$$\frac{dn_e}{dt} = \frac{(1-n_e)}{\tau_{ge}} - \frac{n_e}{\tau_{eg}}.$$

In the steady illumination state the derivative is zero so that

$$\tau_{eg} = \frac{n_e}{(1-n_e)}\tau_{ge}.$$

The excited-state fraction is taken from the analysis of the differential HERFD-XANES spectra, $n_e \approx 0.2$. The number of ground- to excited-state transitions per V atom per unit time is given by

$$\tau_{ge}^{-1} = \Phi\mu(532)/\rho_{\mathrm{V}},$$

in which Φ is the laser fluence ($\Phi \approx 4 \times 10^{19}$ photons $\mathrm{s}^{-1}\,\mathrm{cm}^{-2}$), ρ_V is the density of V atoms ($\rho_V \approx 9.6 \times 10^{20}\,\mathrm{cm}^{-3}$), and $\mu(532)$ the optical attenuation coefficient at $\lambda = 532$ nm ($\approx 7.7 \times 10^3\,\mathrm{cm}^{-1}$), which can be obtained from the diffuse reflectance spectra [13,26]. Using these values, we obtain $\tau_{ge} \approx 3$ ms, from which the lifetime of the trapped state can be estimated as $\tau_{eg} \approx 0.8$ ms.

IV. CONCLUSIONS

In conclusion, by using high-resolution XAS methods we have provided original evidence that photoexcitation (at 532 nm) of V : TiO_2 nanoparticles induces a transfer of electrons from occupied states localized on V dopants to unoccupied states localized on defective Ti cations. In these Ti-related traps, the electrons appear to possess a remarkably long lifetime, which may be a favorable feature for photocatalytic processes. We did not observe any signature of electron transfer from occupied valence states to unoccupied dopant-related states. This does not exclude that such processes occur, but they may be undetectable for essentially two reasons: either the involved states do not have a highly localized character, or the lifetime of the excited state is considerably shorter, precluding its observation by a static differential method. In the near future, time-resolved experiments using an optical pump and an x-ray probe at free-electron laser sources may provide exciting opportunities to unravel the dynamics of photoexcited charge carriers with elemental sensitivity.

ACKNOWLEDGMENT

This research was funded by the Italian Ministry of Research (MIUR) within PRIN-2015 Project No. NEWLI-2015CL3APH.

[1] A. Fujishima, X. Zhang, and D. A. Tryk, Surf. Sci. Rep. **63**, 515 (2008).
[2] R. Jaiswal, N. Patel, D. C. Kothari, and A. Miotello, Appl. Catal. B Environ. **126**, 47 (2012).
[3] T. Umebayashi, T. Yamaki, H. Itoh, and K. Asai, J. Phys. Chem. Solids **63**, 1909 (2002).
[4] J. Osorio-Guillén, S. Lany, and A. Zunger, Phys. Rev. Lett. **100**, 036601 (2008).
[5] W. Zhou, Q. Liu, Z. Zhu, and J. Zhang, J. Phys. Appl. Phys. **43**, 035301 (2010).
[6] J. Choi, H. Park, and M. R. Hoffmann, J. Phys. Chem. C **114**, 783 (2010).
[7] F. Boscherini, in *X-Ray Absorption and Spectroscopy of Semiconductors*, edited by C. S. Schnor and M. C. Ridgway (Springer, New York, 2015).
[8] P. Glatzel and U. Bergmann, Coord. Chem. Rev. **249**, 65 (2005).
[9] L. Amidani, A. Naldoni, M. Malvestuto, M. Marelli, P. Glatzel, V. Del Santo, and F. Boscherini, Angew. Chem. Int. Ed. **54**, 5413 (2015).
[10] G. Rossi, M. Calizzi, V. Di Cintio, S. Magkos, L. Amidani, L. Pasquini, and F. Boscherini, J. Phys. Chem. C **120**, 7457 (2016).
[11] L. Pasquini, M. Sacchi, C. Boelsma, S. Bals, T. Perkisas, and B. Dam, Int. J. Hydrogen Energy **39**, 2115 (2014).
[12] L. Lutterotti, M. Bortolotti, G. Ischia, I. Lonardelli, and H.-R. Wenk, Z. Krist. Suppl. **1**, 125 (2007).
[13] See Supplemental Material at http://link.aps.org/supplemental/10.1103/PhysRevB.96.045303 for Ti K-edge XANES, V valence-to-core XES, and discussion of the optical attenuation coefficient of V : TiO_2 nanoparticles.
[14] V. A. Solé, E. Papillon, M. Cotte, P. Walter, and J. Susini, Spectrochim. Acta Part B Atom Spectrosc. **62**, 63 (2007).
[15] A. Bordage, Propriétés Spectroscopiques et Structure Électronique du Vanadium dans des Matériaux Complexes: Implications Géologiques et Technologiques, Ph.D. Thesis, Université Pierre et Marie Curie - Paris VI, 2009.
[16] M. H. Rittmann-Frank, C. J. Milne, J. Rittmann, M. Reinhard, T. J. Penfold, and M. Chergui, Angew. Chem. Int. Ed. **53**, 5858 (2014).
[17] W. H. Press, S. A. Teukolsky, W. T. Vetterling, and B. P. Flannery, in *Numer. Recipes C* (Cambridge University Press, Cambridge, UK, 2002).
[18] J. Wong, F. W. Lytle, R. P. Messmer, and D. H. Maylotte, Phys. Rev. B **30**, 5596 (1984).
[19] L. Whittaker, T.-L. Wu, C. J. Patridge, G. Sambandamurthy, and S. Banerjee, J. Mater. Chem. **21**, 5580 (2011).
[20] G. A. Waychunas, Am. Mineral. **72**, 89 (1987).
[21] T. L. Hanley, V. Luca, I. Pickering, and R. F. Howe, J. Phys. Chem. B **106**, 1153 (2002).
[22] S. J. Stewart, M. Fernández-García, C. Belver, B. S. Mun, and F. G. Requejo, J. Phys. Chem. B **110**, 16482 (2006).
[23] H. Zhang, B. Chen, J. F. Banfield, and G. A. Waychunas, Phys. Rev. B **78**, 214106 (2008).
[24] V. Luca, S. Djajanti, and R. F. Howe, J. Phys. Chem. B **102**, 10650 (1998).
[25] L. X. Chen, T. Rajh, Z. Wang, and M. C. Thurnauer, J. Phys. Chem. B **101**, 10688 (1997).
[26] D. L. Wood and J. Tauc, Phys. Rev. B **5**, 3144 (1972).